LBL-28370
Preprint

Center for Advanced Materials

CAM

Submitted to Journal of Applied Physics

Laser Heating Effects in the Characterization of Carbon Fibers by Raman Spectroscopy

J.W. Ager III, D.K. Veirs, J. Shamir,
and G.M. Rosenblatt

June 1990

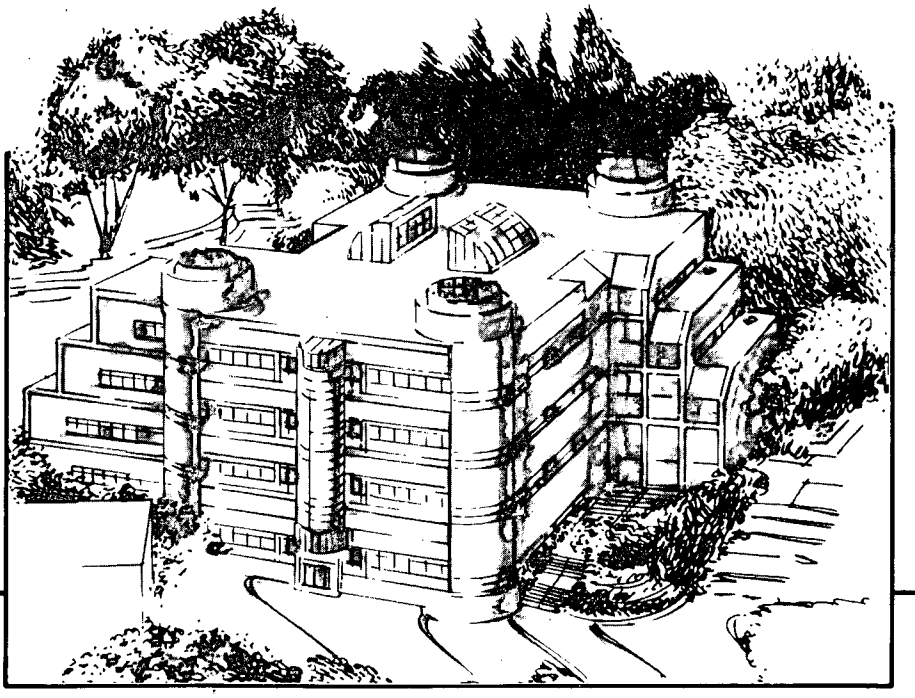

Materials and Chemical Sciences Division

Lawrence Berkeley Laboratory • University of California

ONE CYCLOTRON ROAD, BERKELEY, CA 94720 • (415) 486-4755

Prepared for the U.S. Department of Energy under Contract DE-AC03-76SF00098

LOAN COPY
Circulates
for 2 weeks
Bldg. 50 Library.
Copy 2
LBL-28370

DISCLAIMER

This document was prepared as an account of work sponsored by the United States Government. While this document is believed to contain correct information, neither the United States Government nor any agency thereof, nor the Regents of the University of California, nor any of their employees, makes any warranty, express or implied, or assumes any legal responsibility for the accuracy, completeness, or usefulness of any information, apparatus, product, or process disclosed, or represents that its use would not infringe privately owned rights. Reference herein to any specific commercial product, process, or service by its trade name, trademark, manufacturer, or otherwise, does not necessarily constitute or imply its endorsement, recommendation, or favoring by the United States Government or any agency thereof, or the Regents of the University of California. The views and opinions of authors expressed herein do not necessarily state or reflect those of the United States Government or any agency thereof or the Regents of the University of California.

LBL-28370

Laser heating effects in the characterization of carbon fibers by Raman spectroscopy

Joel W. Ager III, D. Kirk Veirs, Jacob Shamir*, and Gerd M. Rosenblatt

Center for Advanced Materials
Materials and Chemical Sciences Division
Lawrence Berkeley Laboratory
University of California
Berkeley, CA 94720

* Visiting Scientist from Department of Inorganic and Analytical Chemistry, The Hebrew University of Jerusalem, Jerusalem, 91904 Israel.

This work was supported by the Director, Office of Energy Research, U.S. Department of Energy, under contract No. DE-AC03-76SF00098.

Revised version submitted to the Journal of Applied Physics, 6/8/90

Laser heating effects in the characterization of carbon fibers by Raman spectroscopy

Joel W. Ager III, D. Kirk Veirs, Jacob Shamir, and Gerd M. Rosenblatt

Center for Advanced Materials, Materials and Chemical Sciences Division, Lawrence Berkeley Laboratory, University of California, Berkeley, CA 94720.

The first-order Raman spectra of individual 8 μm diameter PAN-derived carbon fibers which had been annealed at five temperatures from 1700°C to 2800°C are measured as a function of incident laser power from 1 to 140 mW. In all fibers studied, the Raman frequencies of the graphite G-band at ca. 1580 cm^{-1} and the disordered-induced D-band at ca. 1360 cm^{-1} shift to lower frequency with increasing laser power. The largest shifts observed before the fiber is physically damaged are about 13 cm^{-1} at a laser power of 30 mW. The band positions decrease further at higher laser power, up to a maximum of about 20 cm^{-1} at 40 mW, and at powers above 30 mW the linewidths and the I_D/I_G intensity ratio change irreversibly as the fiber begins to erode. The irreversible changes extend several hundred μm away from the 2 μm spot illuminated by the laser. The effects are attributed to laser heating. To quantify the degree of laser heating the temperature dependence of the Raman shift (G-band) in pure bulk, highly oriented pyrolytic graphite (HOPG) is measured. To study the heating effect in more detail, a Raman imaging experiment is carried out in which a 0.1 mm spot on a fiber is heated by a focused laser while the fiber is illuminated for Raman characterization along a 1.6 mm length by a low power probe laser. The spatially resolved Raman shifts obtained in this way are combined with the HOPG frequency-temperature calibration to obtain the *in-situ* temperature profile of the laser heated fiber. The measured temperature profile along the fiber is in excellent agreement with a simple convective heat-transfer model. Assuming that the temperature dependence of the G-band position is the same in the fibers as in bulk graphite, the present experiments show that a laser power of 30 mW heats an 8 μm fiber to 330°C and that above 330°C irreversible changes are produced by erosion of the fiber. Unperturbed room-temperature Raman frequencies for the five groups of fibers are obtained by extrapolating to zero laser power.

1 Introduction 6:35 pm June 7, 1990

Carbon fibers are widely used as a structural material in composites because of their high tensile strength-to-weight ratio (up to ten times that of steel). A typical manufacturing technique is to extrude the precursor, typically pitch or polyacrylonitrile (PAN), into a continuous filament. Subsequent heating of the polymeric filament in air at ~1000°C drives off H, O, N, etc. and "carbonizes" the fiber. Annealing in an inert atmosphere at temperatures up to 2900°C (T_{HT} = 2900°C) increases the size and the degree of alignment along the fiber axis of the graphene planes (the two-dimensional hexagonal carbon sheets). Annealed fibers have a higher Young's modulus than unannealed fibers and are known as high modulus or high T_{HT} fibers. The orientation and relative rotation of neighboring, more or less parallel, graphene planes remains random (turbostratic) at all annealing temperatures in ex-PAN fibers. An alternative manufacturing technique is catalytic chemical vapor deposition (CCVD) of a hydrocarbon such as benzene; heat treatment of these fibers to ca. 3000°C results in three dimensional graphitic ordering of the graphene planes. The manufacture, structure, mechanical and physical properties, and analysis of carbon fibers have recently been the subject of a comprehensive review by Dresselhaus et al. [1].

The first-order Raman spectrum of single crystal graphite (e.g., highly ordered pyrolytic graphite or HOPG) consists of a single peak at 1581 cm^{-1} (G-band), corresponding to the doubly degenerate Raman-active E_{2g_2} mode [2]. In all disordered graphites a second peak (D-band) appears near 1355 cm^{-1}. The D-band peak corresponds to a peak in the optical phonon density of states near the Brillouin zone boundary and its intensity arises from relaxation of the $\mathbf{k} = 0$ selection rule caused by breaking the translational symmetry in the disordered material [2] [3] [4]. Both the D- and G-bands appear in the first-order spectra of annealed carbon fibers. The E_{2g_2} mode of HOPG involves the relative in-plane motions of atoms in adjacent planes while the corresponding mode in turbostratic graphite involves only the relative motions of atoms in a single plane. As a result of this distinction, the G-band of turbostratic graphite may appear at a frequency a few cm^{-1} higher than in HOPG [5]. The ratio of the integrated intensities of the D- and G-bands, I_D/I_G, has been

related to the microcrystallite size, L_a, by correlating Raman measurements with X-ray diffraction results [2]. The I_D/I_G ratios of carbon fibers annealed at successively higher temperatures have been shown to decrease steadily, indicating that the average microcrystallite size is larger in fibers annealed at higher temperatures. [6][7][8]

Uniaxial stress and strain also cause changes in the Raman spectra of carbon fibers. Robinson et al. [9] and Galiotis and Batchelder [10] first observed that ~1% strains along the longitudinal axis of a variety of commercial carbon fibers caused the G-band Raman frequency to decrease by up to 15 cm^{-1}. The results recently have been used to map residual stress in carbon fiber composites [11]. Sakata et al. [12] studied quantitatively the effect of uniaxial stress on benzene-derived fibers annealed at 2900°C. They observed that the G-band frequency shifts to lower frequency with increasing tensile stress and that the shift is 3.5 times larger when the laser polarization is parallel to the fiber axis compared to when it is polarized perpendicular to the fiber axis. They used these results to calculate the phenomenological parameters that describe the changes in the spring constant of the $\mathbf{k} = 0$ optical phonons with strain.

In this work we have measured the Raman spectra of individual 8 μm diameter PAN-derived carbon fibers with various T_{HT} as a function of incident laser power from 1 to 140 mW. The G-band frequency shifts to lower frequency with increasing laser power for all fibers studied. The shifts can be up to 20 cm^{-1}, somewhat larger than those observed in the aforementioned mechanical stress and strain experiments. Unperturbed Raman frequencies for the five groups of fibers were obtained by extrapolating to zero laser power. The G- and D-band widths and I_D/I_G ratio remain constant up to laser powers of about 30 mW. Above 30 mW the G- and D-band widths and the I_D/I_G ratios increase. The shift of the G-band Raman frequency was measured as a function of temperature in resistively heated HOPG and used to calibrate the temperature of the carbon fibers. Spatially resolved Raman spectra were obtained along a carbon fiber using a unique imaging Raman apparatus and were used to determine the *in-situ* temperature profile of a laser heated fiber.

2 Experimental

Five groups of PAN-derived fibers were used in the present study with T_{HT} = 1700, 2000, 2400, 2600, and 2800°C [13]. Hereafter in the text, specifying a fiber as 2800 HT means a fiber that was annealed at 2800°C. The graphene planes of ex-PAN fibers have a preferred alignment that is parallel to the fiber axis, but there is typically a wide distribution around this value. The mechanical properties of the fibers are listed in Table 1 [13]. The fibers studied are 8 μm in diameter and all measurements were performed with single fibers.

Figure 1 is an overview of the experimental arrangement. All Raman spectra were excited with the 488 nm line of an Ar^+ laser. A quarter wave plate was used to rotate the laser polarization for polarization studies. In all work reported here, the laser polarization was perpendicular to the fiber axis and all polarizations of the scattered light were collected. In the point-focus experiments a telescope expanded the laser beam to a diameter of 9 mm and a 50 mm coated spherical lens focused the expanded beam onto the fiber. With this optical arrangement the beam waist at the fiber is calculated to be 2 μm. The beam diameter was confirmed to be smaller than the fiber diameter by observing that the laser beam could be completely blocked by the fiber. The laser power was measured between the telescope and focusing lens with an external commercial laser-power meter.

The fibers were carefully mounted by hand on an optical mount with double sticky tape. For the imaging experiments, the fibers were mounted on a rotation stage to facilitate alignment. Most point-focus experiments were performed with the fiber outside the laser focus such that the fiber only partially blocked the beam. This allowed a finer control of the laser power. An iris was used to block all but the central portion of the illuminating laser beam which had a Gaussian profile. The laser power at the fiber was then calculated by measuring the area of the shadow of the fiber compared to the expanded beam area, both observed on a screen located past the laser focus. In a typical

experiment, the image of the laser beam was 65 mm in diameter and the shadow of the fiber was 12 mm in width. In this configuration 24% of the measured laser power is incident on the fiber, assuming a constant laser intensity profile.

For the highly ordered pyrolytic graphite (HOPG) experiments, an oblong sample (2 mm × 2 mm × 5 mm) of HOPG was mounted on two parallel copper rods. The HOPG sample was resistively heated by passing a dc current (up to 20 A at 1 V) through the sample, parallel to the graphite planes. The temperature was measured by a chromel alumel thermocouple pressed against the back of the HOPG sample. The maximum temperature reached in the HOPG experiments was 250°C. Before each set of measurements, fresh basal planes of HOPG were exposed by lifting off graphite layers with adhesive tape. The laser and collection optical axis angles were 50° and 20° from the surface normal, respectively.

The scattered light was collected by a 50 mm f/1.3 camera lens and imaged onto the entrance slit of a 0.64 m single monochromator. An interference filter rejected Rayleigh-scattered light. The dispersed light was detected by an microchannel plate photomultiplier with a position-sensitive resistive anode, the low light level detection and low dark noise advantages of which have been discussed previously [14][15]. With a 1200 groove/mm grating, Raman frequencies from 900 cm^{-1} to 1900 cm^{-1} could be monitored without slewing or scanning the monochromator.

Typical collection times were 300 s. The spectra are corrected for instrument response (mainly the varying transmission of the interference filter) by dividing them by a calibration spectrum obtained with a white light source [16]. Line positions and widths are calculated by fitting the observed spectra to a Lorentzian line shape with a linear background term. There is excellent agreement between the observed and calculated line shapes and the statistical uncertainties of the fit are much smaller than the estimated systematic errors. Line positions are calibrated by comparison with a Ne spectrum [17]. The accuracy of the line center measurements for the G- and D-bands is ±0.8 cm^{-1} and this is our estimate of the systematic errors.

Spatially resolved Raman images were obtained from a 2800 HT fiber using a unique Raman imaging technique that we have described previously [18]. In this technique, a cylindrical lens is used to focus the laser to a line, forming a slit-like illuminated area on the sample. Light scattered from the illuminated area is then imaged onto the entrance slit of the spectrometer. The scattered light entering the slit is dispersed by the spectrometer grating and is projected onto the position sensitive detector (1024 × 1024 pixel format). The height of the entrance slit image projected onto the detector is approximately 800 pixels. Each of these horizontal pixel rows contains the complete Raman spectrum from the corresponding point along the illuminated line on the sample.

In the spatially resolved experiments presented here, the 488 nm laser beam was divided by a beamsplitter. The telescope was removed to reduce the beam diameter and increase the laser power at the sample. One beam (probe) illuminated the sample using a 50 mm cylindrical lens. This formed a ca. 1.6 mm high illuminated area along the 8 μm fiber, which was imaged onto the entrance slit. The second beam (heating) was carefully focused with a 85 mm spherical lens to a 100 μm spot (see Discussion) in the center of the area illuminated by the "probe" beam (see Fig. 1, inset). To maximize spectral resolution in these experiments, we used a 2400 groove/mm grating in the monochromator with a dispersion of 0.4 cm^{-1}/pixel. In the imaging experiments only the G-band at ca. 1580 cm^{-1} was measured.

The probe beam was adjusted to the lowest power possible while still producing enough Raman scattered light in each row to detect and fit in a typical collection time of 10 minutes. Spectroscopic images of the fiber were collected with the probe beam only and with the probe and heating beams both on. To limit the amount of data evaluated, horizontal rows in the spatially and wavelength dispersed image were summed together in groups of four in hardware to yield images with 1024 columns (Raman frequency) and 256 rows (spatial). Analysis of the images was performed using the LBL CHEMMAP computer program [19]. Lorentzian lineshapes were fit to the G-band spectra in each of the 200 spatial rows and the position, FWHM, and peak intensity of the G-band were recorded. The 200 spatial rows analyzed corresponded to 1.6 mm vertical distance

along the fiber. To correct for the curved image of the entrance slit on the exit focal plane of the monochromator, a wavelength calibration image was collected in the following way. The monochromator was slewed such that a Ne emission line was observed at the same horizontal (spectral) position at the center of the detector as the HOPG G-band, and an image was collected and fit. Shifts in the G-band frequency as a function of vertical position were calculated as differences between the G-band frequency and the Ne calibration frequency in each spatial row.

3 Results

3.1 Carbon fibers - point-focus measurements

Typical point-focus spectra are shown in Fig. 2 for a 2000 HT and a 2800 HT fiber. The G- and D-bands narrow and the I_D/I_G ratio decreases with increasing T_{HT}. These change have been documented previously [6-8]. They are attributed to an increase in the graphite microcrystallite size (in-plane coherence length), L_a, with increasing annealing temperature [6].

Figure 3 shows the Raman scattering intensity of the G- and D-bands, the G- and D-band positions and widths, and the I_D/I_G ratio for a 2800 HT fiber as a function of illuminating laser power. The laser power at the fiber varied from 0.6 to 140 mW in the 30 experiments shown. We have divided the laser heating effects into five phenomenological regions (Table II) and these are indicated in Fig. 3.

Looking first at the scattering intensities, in region I (0 - 30 mW laser power incident on the fiber), the scattering intensity increases linearly with laser power, as expected for ordinary Raman scattering. In region II (30 - 40 mW), the increase is still linear but occurs at a faster rate. In region III (40 - 55 mW), the scattering intensity is roughly constant as the incident laser power increases. In region IV (55 - 90 mW) the total intensity decreases with increasing laser power. In region V (90 - 140 mW) the Raman intensity is again constant. By this point the fiber is nearly completely destroyed. Figure 4 is a micrograph of the fiber taken after this series of experiments; at least 90% of the material in the laser focus had been eroded.

The Raman frequencies, linewidths, and relative intensities also change with increasing laser power. Figure 5 shows two spectra from the same 2800 HT fiber, collected at 1.7 mW and 51 mW laser power. The Raman intensity is normalized to the laser power. Both the G- and D-bands are shifted to lower frequency and I_D/I_G ratio is larger in the lower spectrum, taken at the higher laser power. Now return to Figs. 3(b)-(d) which summarize the changes in the experimental observables for a 2800 HT fiber as a function of laser power. In regions I and II, the G- and D-band frequencies decrease monotonically with increasing laser power. The frequencies then remain roughly constant upon further increases in the incident laser power. In region I the I_D/I_G ratio and FWHM of the G- and D-bands are constant. In region II the I_D/I_G ratio and both linewidths increase sharply. In region III the I_D/I_G ratio drops slightly and line widths remain constant. Both the I_D/I_G ratio and the line widths remain constant in regions IV and V.

Figure 3 also shows the results of an experiment carried out to determine the reversibility of the observed changes in the Raman spectrum. After a series of experiments in which the power incident on the fiber was increased to 50 mW (Region III), a spectrum was collected at 8 mW. The G-band frequency shifts are reversible and the D-band shifts nearly so, i.e., the lines return close to their original positions upon lowering the laser power. However, changes in the I_D/I_G ratio and G-band FWHM are irreversible in that if the laser power is in a region where changes occur and is subsequently reduced to a value in region I, the I_D/I_G ratio and G-band FWHM do not return to their original values.

Subsequently, we measured Raman spectra at low laser power (8 mW) at several longitudinal positions along this fiber away from the region where the laser had removed over 90% of the fiber. As shown in Fig. 6, permanent increases in the I_D/I_G ratio extend in both directions for several hundred μm from the damaged area, a distance orders of magnitude larger than the diameter (ca. 2 μm) of the illuminating laser beam during damage. The magnitude of the increase in the I_D/I_G ratio diminishes with distance away from the damaged area. Referring back to Fig. 4, increases in the I_D/I_G ratio are measured in regions of the fiber where no damage was observed by optical microscopy.

We measured the G- and D-band frequency shifts as a function of laser power in Region I for all five groups of fibers. In this region the G- and D-bands shift linearly to lower frequency with increasing laser power while the widths and the I_D/I_G ratio remain constant. Figure 7 show the G-band shifts as a function of laser power at the fiber for single experiments with individual 1700 HT, 2000 HT, and 2600 HT fibers. The laser power dependences of the G- and D-band positions are summarized in Table III for the five different heat treatment temperatures. Table III also summarizes room-temperature peak positions, obtained by extrapolation to zero laser power as illustrated in Fig. 7.

3.2 Carbon fibers - imaging Raman

Imaging Raman data were obtained using a low power probe beam, which illuminated the fiber through a cylindrical lens and a variable power heating beam which was focused to a small spot on the fiber; cf. Fig. 1 inset. The G-band positions (calibrated to a Ne line as described above) measured with the probe beam only and with the probe plus heating beams shown in Fig. 8. The extrapolated room temperature position of the G-band from a 2800 HT fiber with no laser heating is 1584.1 cm^{-1}, cf. Table II.

The 45 mW probe laser lowers the G-band frequency about 4 cm^{-1} from the extrapolated room-temperature value along the entire length of the probed region, Fig. 8. The data show very little variation (less than ± 1 cm^{-1}) in the band position over the 1.5 mm probed length of the fiber. When the heating beam is turned on, a further frequency decrease of ca. 20 cm^{-1} (for a heating beam of 280 mW) is observed in the center of the illuminated region. The G-band frequency returns to the value measured without the heating beam at distances about 500 μm below and about 700 μm above the point illuminated by the heating laser. The asymmetry of the Raman frequency around the illumination point arises from convective cooling and the vertical alignment of the fiber, as discussed below.

The measured intensities of the G-band along the fiber are shown in Fig. 9. These intensities are proportional to the laser power at each position along the fiber for the two experiments. The peaks in the G-band intensity above and below the large heating laser peak are due to additional illumination spots arising from secondary reflections from the beam splitter. The peak above the main illumination point is smaller then the peak below the illumination point because it arises from a weaker reflection off the back of the beam splitter. The spot size of the heating laser beam is ca. 100 μm. The probe and heating beam powers were 45 and 280 mW, respectively, in the experiment shown. We were not able to measure precisely the laser power impinging on the fiber as we did for the point-focus measurements. However, the beam waist is much larger than the 8 μm fiber diameter and only some portion of the heating beam hits the fiber. The larger beam waist arises from the removal of the telescope.

3.3 Highly Ordered Pyrolytic Graphite

The first-order Raman spectrum of HOPG consists of a single line at 1581 cm^{-1}. The position of this peak was measured as a function of temperature for temperatures between 20°C and 250°C. The peak position and width of the G-band were determined by fitting a Lorentzian line shape to the observed data. When the sample was heated, the position of the G-band shifted to lower frequency (Fig. 10). The linewidth remained constant during these experiments. The peak returned to its original room temperature position when the sample was cooled, as was observed with the fibers. The maximum frequency shift observed was 8 cm^{-1}. The relation between Raman frequency and temperature appears linear over the T range studied; the slope of a linear least squares fit to the data is 0.034 cm^{-1}/K or 30 K/cm^{-1}.

4 Discussion

Both increasing the laser power in the fiber experiments and increasing the temperature in the bulk graphite experiments causes the G-band to shift to lower frequency (Figs. 3, 7, and 10). We show in the next section that the spatial distribution of the frequency shift of the G-band along

the fiber and away from the heating laser focus, shown in Fig. 8, is in excellent agreement with a simple heat transfer model. The shift in the positions of the G- and D-bands observed in the Raman spectra of the carbon fibers with increasing laser power is attributed to heating of the fibers.

The frequency shifts measured as a function of temperature for the HOPG G-band can be used to calculate the temperature of the fibers. As seen in Fig. 10, the G-band of HOPG has decreased about 7 cm^{-1} at a temperature of 250°C. The maximum G-band frequency shifts observed in the carbon fibers were about 20 cm^{-1} (Fig. 3). If we assume that the frequency shift as a function of temperature is the same for HOPG and the fibers, the temperature is computed to be about 600°C at the point where the Raman frequency shift of the fiber is a maximum (the end of region III, cf. Fig. 3).

Table II summarizes the experimental observations in the five phenomenological regions identified in Fig. 3. It is significant that the various shifts for the G- and D-bands track each other (Fig. 3). A plausible interpretation is as follows. In region I the temperature increase due to laser heating causes strains that change the elastic constants of the E_{2g} mode and shift the G-band to lower frequency. Similar changes presumably also occur in the D-band elastic constants. Since the I_D/I_G ratio and the width of the G- and D-bands remain constant in Region I, we infer that the fiber microcrystalline structure in the volume probed by the laser, including the average microcrystallite size L_a, does not change in this region.

In region II, further increases in the fiber temperature continue to change the elastic constants and the frequency shifts continue, but L_a in the probed volume decreases as reflected by increases in the I_D/I_G ratio and the linewidths. The decrease of the average microcrystallite size does not appear to be caused by the temperature induced strains; no changes in the I_D/I_G ratio or the linewidths are observed upon heating HOPG. In addition, the fibers have been annealed in an inert atmosphere at temperatures much higher than those produced by the laser; higher annealing temperature decrease the I_D/I_G ratio and the linewidths. One possibility for the changes observed in Region II is that erosion removes the skin layer of the fiber, exposing a less ordered fiber core. Annealed

PAN-derived fibers are known to have the graphene planes near the surface aligned parallel to the fiber surface and to be quite disordered near their cores [1]. This is consistent with the experimental observation that changes in the I_D/I_G ratio and the line widths are irreversible. In Region II the rate at which the Raman scattered intensity increases with laser power is greater than in Region I. This may be due to erosion and roughening increasing the surface area exposed to the laser; this would increase the effective probe volume (the optical skin depth of the laser radiation is ca. 60 nm [6]) and hence the scattered intensity.

In Region III the frequency shifts do not continue their downward trend, presumably because the temperature no longer increases. At the beginning of this region, perhaps half of the diameter of the fiber has been eroded and additional laser power produces further erosion, decreasing the effective probe volume. The decrease in scattering volume balances the increasing laser power and leads to the nearly constant scattering intensity observed in Fig. 3. In region IV, severe erosion of the fiber occurs, leading to a decrease in scattered intensity. In region V, almost all the material in the laser focus has been eroded and the observed Raman scattering comes from material at the edges of the Gaussian laser beam profile.

These experiments show that to obtain a room temperature measurement of the G- and D-band positions in fine carbon fibers very low laser powers must be used. For example, the band positions listed in our preliminary report on these fibers [8] are shifted to frequencies 6-20 cm^{-1} below their room temperature values by laser heating. In this work, we have linearly extrapolated the results for all the fibers to zero laser power and list these frequencies in Table II. In Fig. 11, we graph the room-temperature G-band frequency determined in this way vs. T_{HT}. The G-band frequency decreases with increasing T_{HT}, approaching that of HOPG for the 2400 HT, 2600 HT, and 2800 HT fibers.

It is interesting that the trend seen with the ex-PAN fibers parallels that reported previously by Chieu et al. [6] for benzene-derived CCVD fibers; their data are also shown in Fig. 11. The G-band frequency observed is higher in the lower HT fibers because relaxation of the $k = 0$ selection

rule in the lower HT fibers brings in some of the high frequency mid-zone phonons near 1620 cm^{-1} [6]. The small systematic differences (~3 cm^{-1}) between the two sets of data reflect differences between the ex-PAN and CCVD fibers studied in the two experiments. One difference is that the I_D/I_G ratios of the ex-PAN fibers are higher than those of the CCVD fibers annealed at the same temperature. Recalling that the I_D/I_G ratio has been empirically correlated to L_a (in-plane microcrystallite size) [2][4], Fig. 12 compares the G-band positions of ex-PAN and CCVD fibers with similar in-plane microcrystallite sizes. The G-band frequency correlates similarly with the I_D/I_G ratio in both groups of fibers, suggesting that the two types of fibers reach a given in-plane microcrystallite size at different annealing temperatures. On the other hand, another difference between the two types of fibers is that the ex-PAN fibers are turbostratic while the CCVD fibers exhibit three dimensional ordering. Because of the distinction between single-layer in-plane mode of turbostratic graphite and the E_{2g_2} mode of single-crystal graphite, which involves atoms in adjacent planes, the G-band frequency of turbostratic graphite appears to lie a few wavenumbers above that of single crystal graphite [5]. Thus, the frequency differences between the two groups of fibers may arise from differences in inter-plane ordering rather than, or in addition to, in-plane crystallite size.

Figure 13 is a graph of the dependence upon laser power of the G- and D-band frequencies (the slopes of the lines in Fig. 7) vs. T_{HT}. Although there is scatter in the data, two trends are evident. The first is that the changes in the G-band position, for a given laser power, are larger than those of the D-band. The magnitude of the temperature induced shift appears to be roughly proportional to the frequency of the band. The second is that the laser-power dependences of both bands are larger for the lower T_{HT} fibers. This may be due to the differing thermal conductivities of the fibers. Since the thermal conductivity of the fibers is limited by scattering from defects, crystal imperfections, and microcrystallite boundaries, fibers with a larger L_a (and/or a larger measured I_D/I_G ratio) have a larger thermal conductivity [20]. The G- and D-band temperature shifts might be larger for the lower T_{HT} fibers because these have a lower thermal conductivity and thus reach

a higher temperature at a given laser power than do the higher T_{HT} fibers. For example, based on the HOPG G-band temperature dependence, the heating of the 1700 HT fiber is 23 K/mW and that of the 2800 HT fiber is 10 K/mW in Region I.

The carbon fibers used in this study are too small ($d = 8$ μm) to use conventional temperature measurement methods such as optical pyrometry. Assuming that the shift of the G-band with temperature is the same in the fibers as in HOPG, the frequency shifts observed in the Raman profile in Fig. 8 can be used to compute the temperature profile. The result is shown in Fig. 14. We estimate that the maximum temperature attained in the heat-probe experiment is 720°C. The temperature distribution has a FWHM of about 500 μm.

The experimental data in Fig. 14 can be fit with a simple, one-dimensional model of the temperature distribution of a horizontal cylindrical system assuming a point heating source and free conductive cooling. The fiber thermal conductivity and absorbed laser power are variable parameters in a least squares fit. The model is described in the Appendix. The results of the fit are a fiber thermal conductivity of 1.1 W cm^{-1} K^{-1} and an absorbed laser power of 20 mW. The temperature profile calculated using these results is shown in Fig. 14. In spite of the simplifications in the model (e.g., the thermal conductivity of the carbon fibers is known to be T dependent), the agreement with the data is excellent. The measured profile also shows an expected asymmetry due to the vertical alignment of the fiber, in that the fiber is slightly warmer than the model above the heating laser focus (positive position) and slightly cooler below the focus (negative position). PAN-derived fibers with a similar I_D/I_G ratio to the 2800 HT fiber used in this experiment were found by Heremans et al. [20] to have thermal conductivities of about 1 W cm^{-1} K^{-1}, in good agreement with the value obtained here. In addition, the laser power absorbed by the fiber of 20 mW obtained in the fit is in agreement with the value expected from the beam spot size of 100 μm estimated from the G-band intensity measurements (Fig. 9) and the emissivity ($\varepsilon \approx 0.6$).

5 Conclusions

The laser power dependence of the Raman spectra of high T_{HT} (high modulus) PAN-derived carbon fibers has been studied. In all fibers studied, the Raman frequency of the G- and D-bands shift to lower frequency with increasing laser power. The maximum G-band shifts that are observed before the fiber is physically damaged are about 13 cm^{-1} at a laser power of 30 mW. The band positions continue to shift up to a maximum of about 20 cm^{-1} at 40 mW, and the linewidths and the I_D/I_G ratio change irreversibly as the fiber erodes.

The observed shifts in the Raman band positions of the fibers are attributed to strains caused by laser heating of the fiber. Temperature increases in the laser focus on the order of a few hundred up to 700°C are computed by calibrating with measurements of the G-band frequency shift in HOPG as a function of temperature. Even a laser power as low as 10 mW causes a temperature increase of ca. 100° and a G-band shift of ca. 3.5 cm^{-1} in a 2800 HT ex-PAN fiber. The observations show that reproducible room-temperature characterization of the bonding and microstructure in fine carbon fibers by Raman spectroscopy must be carried out at very low incident laser power and/or by extrapolating measurements back to zero laser power. Upon doing this, the present experiments yield results that are in good agreement with previous studies that used similarly annealed fibers. For example, for the fibers studied here, the G-band frequency and the I_D/I_G ratio both decrease with increasing heat treatment temperature. In addition, the I_D/I_G ratio may be larger in the interior of the fiber than in the surface layer.

The problem of laser heating is general in laser studies of small fibers and the magnitude of the effect depends on the thermal conductivity of the fibers. The effect will be least important for fibers with a very high longitudinal thermal conductivity. Benzene CCVD fibers, for example, have a thermal conductivity 20× that of ex-PAN fibers and thus can be subjected to about 20× the laser power for the same degree of heating and associated effects. The PAN-derived carbon fibers

studied here represent an intermediate case. The heating effect will be larger in fibers which have a smaller longitudinal thermal conductivity; for example, the thermal conductivity of SiC fibers is 1/10 that of ex-PAN carbon fibers.

Finally, for the first time (to our knowledge) an in-situ temperature profile measurement has been measured for a single carbon fiber. The observed temperature profile is in excellent agreement with a simple heat transfer model. Possible further applications of Raman imaging include the non-destructive in-situ observation of temperature or stress in carbon and graphite composite materials.

6 Acknowledgements

We thank E. Fitzer and F. Künkele of Universität Karlsruhe for suggesting to us the possibility of laser heating during Raman characterization of carbon fibers and for supplying the fibers, M. Dresselhaus of MIT for helpful suggestions on the manuscript, H. Lee and E. Loucks for developing data acquisition and analysis software, and M. Salmeron for providing the HOPG sample. This work was supported by the Director, Office of Energy Research of the U.S. Department of Energy, under contract No. DE-AC03-76SF00098.

7 Appendix - heat transfer model

The one-dimensional T profile of the fiber under laser heating can be estimated following essentially a textbook approach used for heat transfer in one-dimensional fins. The model has the laser as the heat source and free convective cooling as the heat sink. In steady state, the continuity equation for one-dimensional heat flux is [21]:

$$\frac{I_{laser}(x)}{2} - 2h(T - T_{air}) = -K_{fiber} r_{fiber} \frac{d^2T}{dx^2} \tag{A1}$$

where x is the distance along the fiber and $x = 0$ at the laser focus, I_{laser} is the absorbed laser power, h is the coefficient for free convective cooling, r_{fiber} is the radius of the fiber (4 μm), T is the temperature of the fiber, T_{air} is the ambient air temperature (300 K), and K_{fiber} is the thermal

conductivity of the fiber. Although the thermal conductivity is a function of T and, therefore, of x, a single value is employed for simplicity. Half the absorbed laser power is taken as the heat source, since the other half of the absorbed power is dissipated by propagation in the -x direction. Radiative cooling of the fiber is negligible at the temperatures attained in these experiments. Since, as shown below, the thermal gradient is small over the extent of the beam waist, we use a flux boundary condition at $x = 0$ corresponding to half the total absorbed laser power, i.e., $I_{laser}(x) = 0.5 I_{laser}\delta(x)$, where I_{laser} is the total laser power absorbed by the fiber. The other boundary condition is

$$\left.\frac{dT}{dx}\right|_{x=L} = 0 \tag{A2}$$

where L is an scaling length discussed below. The solution to Eq. (1) with these boundary conditions is:

$$T'(x) = \left(\frac{\exp(-ml)}{2\sinh(ml)}\exp(mx) + \frac{\exp(ml)}{2\sinh(ml)}\exp(-mx)\right)\frac{I_{laser}}{mK_{fiber}\pi r_{fiber}^2} \tag{A3}$$

where the temperature increase, T', is defined

$$T'(x) = T(x) - T_{air}$$

and

$$m = \left(\frac{2h}{K_{fiber} r_{fiber}}\right)^{0.5}.$$

The solution is insensitive to the value of L as long as $L > 3/m$.

The coefficient for free convective cooling, h, is estimated using empirical relations for horizontal cylindrical system found in the literature. The Grashof number is defined [22]:

$$N_{Gr} = \frac{(2r_{fiber})^3 \rho_{air}^2 \beta g (T_1 - T_2)}{\mu_{air}^2} \tag{A4}$$

where T_1 and T_2 are the fiber and air temperatures, 500 K and 300 K in these calculations. The temperature at which the gas properties should be calculated, T_f, is defined as $0.5(T_1 + T_2)$. The final value of h is insensitive to the values of T_1, T_2, and T_f over the range expected in this experiment. The rest of the variables in Eq. (5) are:

$\rho_{air} = \frac{30 \quad \text{gm}}{22.4 \quad 1}\left(\frac{298}{T_f}\right)$, the density of air,

$\beta = \frac{1}{T_2}$, the coefficient of thermal expansion for ideal gases,

$g = 9.8$ m s^{-1}, the acceleration of gravity, and

$\mu_{air} = 227\times10^{-6}$ gm cm^{-1} s^{-1}, the viscosity of air at 400 K; all values are well known.

These values yield $N_{Gr} = 6.6\times10^{-6}$. We now calculate the Rayleigh number:

$$N_{Ra} = N_{Gr} N_{Pr}, \tag{A5}$$

where N_{Pr} is the Prandtl number and is 0.706 for air below 900 K.

We follow Lienhard [21] in empirically relating the Nusselt number to the Rayleigh number:

$$N_{Nu} = \left(0.60 + 0.387\left(\frac{N_{Ra}}{(1+(0.559/N_{Pr})^{9/16})^{(16/9)}}\right)^{1/6}\right)^2 \tag{A6}$$

Finally, we relate the coefficient for free conduction, h, to the Nusselt number:

$$h = \frac{K_{air}}{2r_{fiber}} N_{Nu}, \tag{A7}$$

where K_{air} is the thermal conductivity of air and is 326×10^{-6} W cm^{-1} K^{-1} at 400 K. Using Eqs. (A4) - (A7), $h = 0.168$ J cm^{-2} s^{-1} K^{-1} for an 8 μm fiber. Using this value of h in Eq. (A3), I_{laser} and K_{fiber} are the only remaining unknowns. These are taken as variable parameters in the fit of the data to Eq. (A3).

References

1. M.S. Dresselhaus, G. Dresselhaus, K. Sugihara, I.L. Spain, H.A. Goldberg, *Graphite Fibers and Filaments* (Springer-Verlag, Heidelberg, 1988).

2. F. Tuinstra and J.L. Koenig, J. Chem. Phys **53**, 1126 (1970).

3. R.J. Nemanich and S.A. Solin, Phys. Rev. B **20**, 392 (1979).

4. P. Lespade, R. Al-Jishi, and M.S. Dresselhaus, Carbon **20**, 427 (1982).

5. M.S. Dresselhaus, private communication, 1990.

6. T.C. Chieu, M.S. Dresselhaus, and M. Endo, Phys. Rev. **B 26**, 5867 (1982).

7. E. Fitzer, E. Gantner, F. Rozploch, and D. Steinert, High Temperatures-High Pressures **19**, 537 (1987).

8. G.M. Rosenblatt and D.K. Veirs, High Temp. Sci., in press.

9. I.M. Robinson, M. Zakikhani, R.J. Day, R.J. Young, and C. Galiotis, J. Mat. Sci. Let. **6**, 1212 (1987).

10. C. Galiotis and D.N. Batchelder, J. Mat. Sci. Let **7**, 545 (1988).

11. C. Galiotis, N. Melanitis, D.N. Batchelder, I.M. Robinson, and J.A. Peacock, Composites **19**, 321 (1988); R.J. Young, R.J. Day, M. Zakikhani, and I.M. Robinson, Composites Sci. Tech. **34**, 243 (1989).

12. H. Sakata, G. Dresselhaus, M.S. Dresselhaus, and M. Endo, J. Appl. Phys. **63**, 2769 (1988).

13. The fibers were provided by Professor E. Fitzer, Universität Karlsruhe. A detailed description of their manufacture is found in E. Fitzer and W. Frohs in *Carbon 88, Proceedings of an International Conference on Carbon*, (Institute of Physics, London, 1988), pp. 298-300 and in E. Fitzer and F. Künkele, *ibid.*, pp 488-490.

14. D.K. Veirs, V.K.F. Chia, and G.M. Rosenblatt, Appl. Opt. **26**, 3530 (1987).

15. W.P. Acker, B. Yip, D.H. Leach, and R.K. Chang, J. Appl. Phys. **64**, 2263 (1988).

16. Our white light source was an incandescent light bulb. The variation of the emission intensity of the lamp over the observed wavelength region introduces a small systematic bias in the measurement of relative intensities. For example, for a lamp color temperature of 2700 K, the intensity ratio for the wavelengths that correspond to 1600 cm^{-1} and 1300 cm^{-1}, I_{1600}/I_{1300}, is 1.08. The reported I_D/I_G ratios were corrected for this effect.

17. *American Institute of Physics Handbook*, edited by D.E. Gray (McGraw-Hill, New York, 1963) pp. 7-48 - 7-55.

18. D.K. Veirs, G.M. Rosenblatt, R.H. Dauskardt, and R.O. Ritchie, in *Microbeam Analysis*, ed. D.E. Newbury (San Francisco Press, San Francisco, 1988) pp. 179-181; R. Dauskardt, D.K. Veirs, and R.O. Ritchie, J. Am. Ceram. Soc. **72**, 1124 (1989); D.K. Veirs, J.W. Ager III, E.T. Loucks, and G.M. Rosenblatt, Appl. Opt., in press.

19. E.T. Loucks and D.K. Veirs, computer code CHEMMAP, (copyright 1990, Lawrence Berkeley Laboratory, University of California).

20. J. Heremans, I. Rahim, and M.S. Dresselhaus, Phys. Rev. B **32**, 6742 (1985).

21. J.H. Lienhard, *A Heat Transfer Textbook*, (Prentice-Hall, Englewood Cliffs, New Jersey, 1987), pp. 132-143.

22. M. Jakob and G.A. Hawkins, *Elements of Heat Transfer*, (Wiley, New York, 1957), p. 122.

Table I. Mechanical and electrical properties of the PAN-derived carbon fibers used in this work. The data are from ref. 13.

T_{HT} (°C)	Tensile strength (MPa)	Young's modulus (GPa)	Resistivity 10^{-3} Ω-cm
1700	3500	250	1.3
2000	2500	270	1.1
2400	2200	290	-
2600	1700	310	-
2800	1300	320	-

Table II. Characterization of different regimes in the laser heating of a 2800 HT carbon fibers. The experimental observables are for increasing laser power.

Laser heating region	Intensity of G- and D-bands	Raman frequency shift of G- and D-bands (reversible)	FWHM of G- and D-bands (irreversible)	I_D/I_D ratio (irreversible)	Interpretation
Region I 0 - 30 mW	linear increase	decreases	constant	constant	Temperature increase causes strains, microcrystallite size (L_a) and disorder are unchanged
Region II 30 - 40 mW	linear increase at a faster rate than in Region I	decreases	increases	increases	Oxidative erosion exposes the interior of the fiber; strain continues to increase.
Region III 40 - 55 mW	constant	constant	constant	slight decrease then constant	Maximum strain reached, erosion extends beyond the center of the fiber
Region IV 55 - 90 mW	sharply decreases	constant	constant	constant	Continued erosion of the fiber; decreasing amounts of material exposed to the laser beam.
Region V 90 - 140 mW	constant	constant	constant	constant	Fiber is almost totally eroded in the laser focus, signal from edges of laser beam
Experimental observable sensitive to:	laser power and amount of material	temperature	L_a and/or disorder	L_a and/or disorder	

Table III. Summary of laser power dependence of the G- and D-band frequencies. Tabulated room-temperature G- and D-band frequencies are from extrapolation to zero laser power. The results for the 2800 HT fiber are an average of three experiments with different fibers; all other results are from single experiments.

T_{HT} (°C)	G-band frequency (cm^{-1})	D-band frequency (cm^{-1})	I_D/I_G ratio	G-band laser power dependence (cm^{-1}/mW)	D-band laser power dependence (cm^{-1}/mW)
1700	1589.9	1356.9	1.6	-0.76	-0.48
2000	1590.2	1358.4	1.1	-0.49	-0.35
2400	1585.7	1357.4	0.77	-0.32	-0.23
2600	1585.9	1360.8	0.55	-0.36	-0.27
2800	1584.1	1360.5	0.45	-0.35	-0.33

Figure Captions

Fig. 1 Overview of experimental apparatus and (inset) sample geometry for imaging experiments

Fig. 2 First-order Raman spectra of (a) 2000 HT and (b) 2800 HT PAN-derived carbon fibers. The prominent features are the graphite G-band at ca. 1580 cm^{-1} and the disorder-induced D-band at ca. 1360 cm^{-1}. The laser power was 15 mW.

Fig. 3 Laser power dependence of the carbon G-band (closed squares) and D-band (open squares) for a 2800 HT fiber: a) Total integrated scattered intensity (the displayed values have been divided by 1000); b) Raman frequencies; c) linewidths; d) I_D/I_G ratio. All values graphed vs. laser power at the fiber. The collection time was 300 s. Diamonds correspond to values measured after first increasing the laser power to 50 mW. The different regions labelled with Roman numerals are summarized in Table I and discussed in the text.

Fig. 4 Micrograph of a damaged 2800 HT fiber after the series of experiments shown in Fig. 3. The diameter of the fiber is 8 μm. The laser beam was incident from the right hand side of the photograph.

Fig. 5 Raman spectra of a 2800 HT carbon fiber at 1.7 mW (upper trace) and 51 mW (lower trace) laser power. The spectra correspond to data from Regions I and III in Fig. 3, respectively. The intensities are normalized to the laser power and the upper trace is offset by 100 counts mW^{-1}. The shift of both the G- and D-bands to lower Raman frequency and the increase of the I_D/I_G ratio are apparent in the spectrum obtained at the higher laser power.

Fig. 6 Measurement of the I_D/I_G ratio as a function of distance from the damaged spot for the fiber shown in Fig. 4. Increases in the I_D/I_G ratio, indicative of permanent changes in the fiber, are seen several hundred μm from the laser focal point, in regions where no damage was observed by optical microscopy.

Fig. 7 Carbon G-band frequency as a function of incident laser power for individual ex-PAN fibers: 1700 HT fiber (triangles), 2000 HT fiber (squares), and 2600 HT fiber (circles). The lines are least squares fits. The uncertainties in the frequencies are ±0.8 cm^{-1}.

Fig. 8 The frequency of the G-band as a function of vertical position along the fiber: probe laser beam only (upper trace) and probe and heating beams (lower trace). Positive positions correspond to points above the laser focus. The collection time for each trace was 10 minutes.

Fig. 9 The intensity of the G-band as a function of vertical position along the fiber: probe beam only (lower trace) and probe and heating beams (upper trace). Same experiment as Fig. 8.

Fig. 10 The dependence of the first-order G-band frequency of HOPG upon T. The line is a linear least squares fit with a slope of 0.034 cm^{-1}/K. The error bars are the estimated systematic error.

Fig. 11 G-band frequency for PAN-derived carbon fibers obtained from extrapolation to zero laser power as a function of T_{HT} (open circles). Data of Chieu et al. [6] for benzene CCVD fibers (closed circles).

Fig. 12 G-band frequency vs. I_D/I_G ratio: (open circles) PAN-derived fibers, this work; (closed circles) benzene CCVD fibers, data of Chieu et al. [6].

Fig. 13 Laser power dependence of the G-band (closed squares) and D-band (open squares) frequencies vs. T_{HT}. Power dependencies are determined by linear least squares fits to plots of band frequency vs. laser power (cf. Fig. 7).

Fig. 14 *In-situ* temperature profile of a 2800 HT fiber determined from the measured G-band frequency as a function of vertical position along the fiber (cf. Fig. 8). The solid line is a fit to a simple heat transfer model (see Appendix) with a laser power absorbed by the fiber of 20 mW and a fiber thermal conductivity of 1.1 W cm^{-1} K^{-1}.

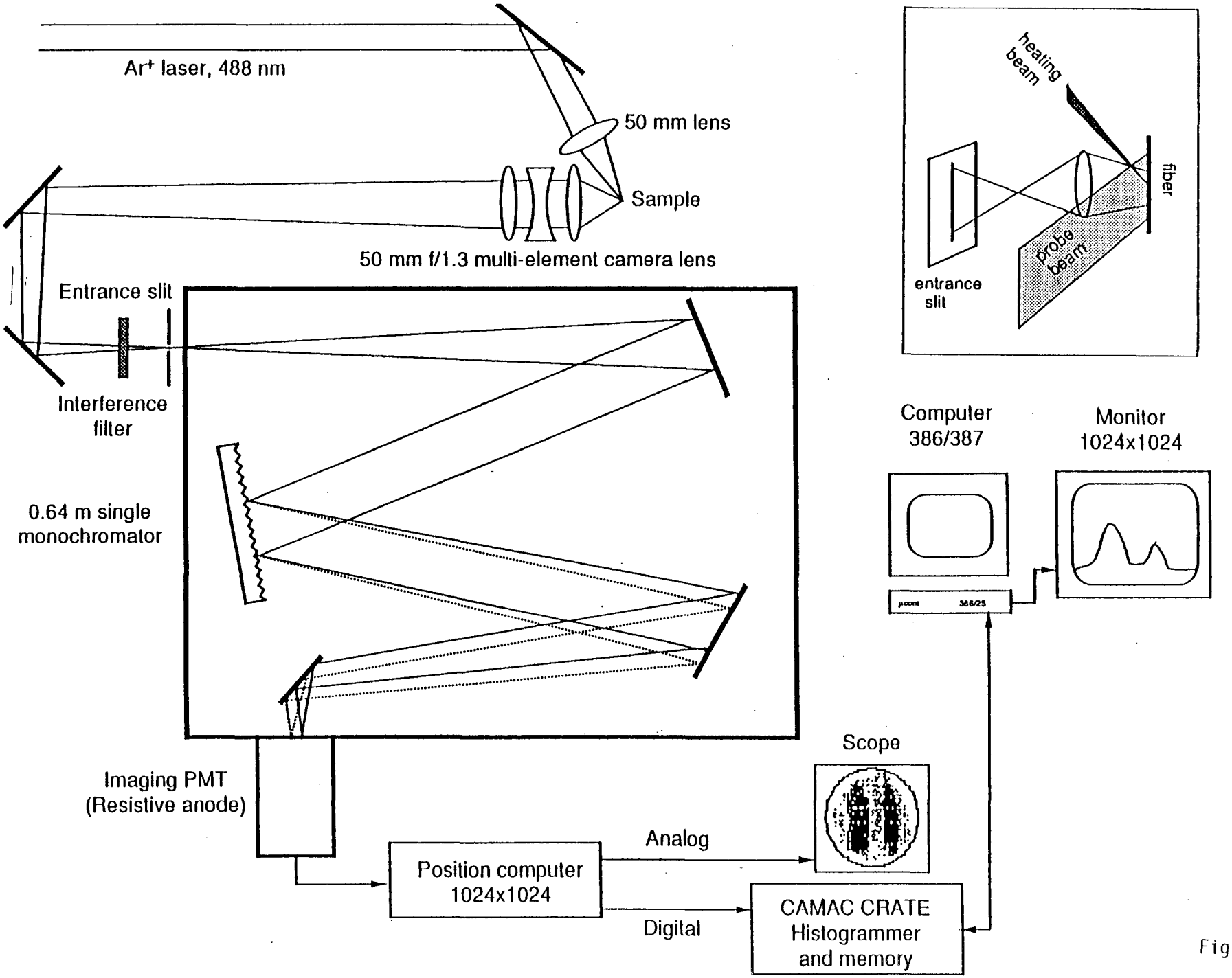
Ar+ laser, 488 nm
50 mm lens
Sample
50 mm f/1.3 multi-element camera lens
Entrance slit
Interference filter
0.64 m single monochromator
Imaging PMT (Resistive anode)
Position computer 1024x1024
Analog
Digital
Scope
CAMAC CRATE Histogrammer and memory
Computer 386/387
Monitor 1024x1024
heating beam
fiber
probe beam
entrance slit

Fig. 1

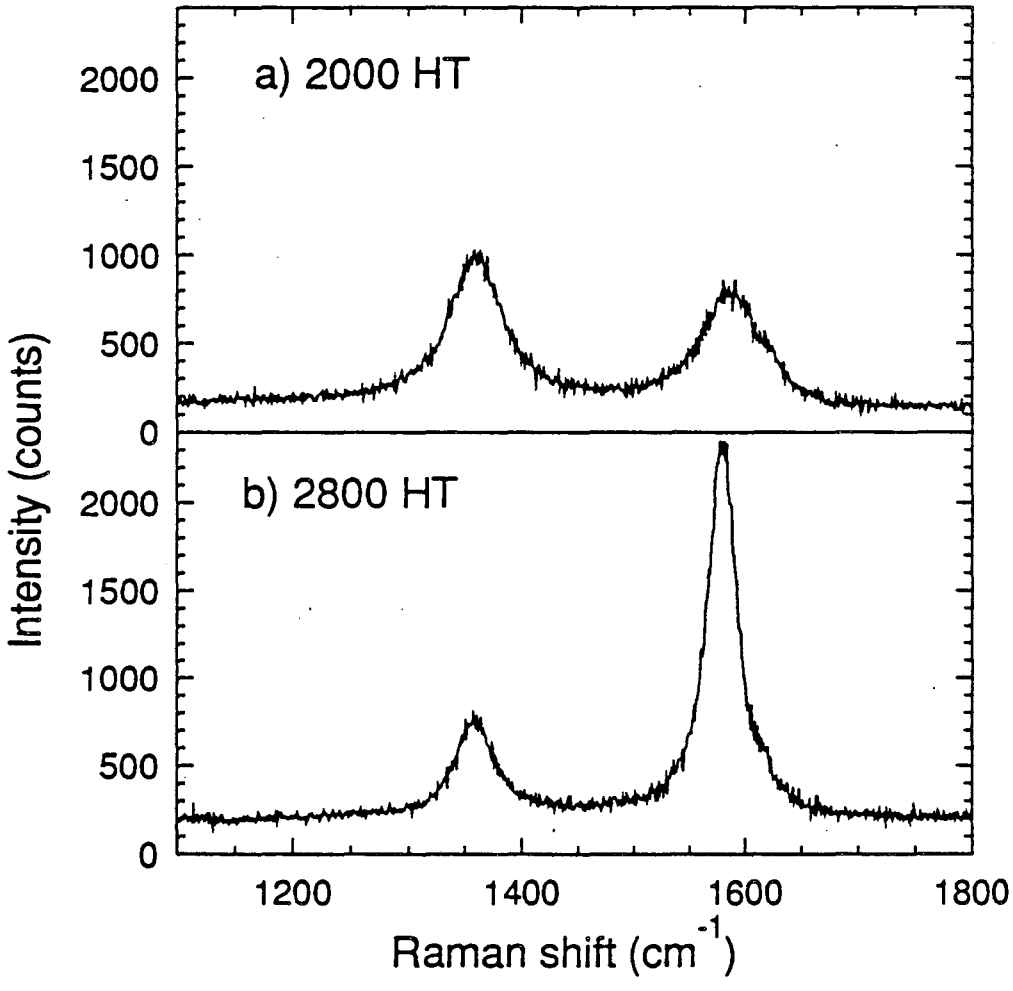
a) 2000 HT
b) 2800 HT
Intensity (counts)
2000
1500
1000
500
0
2000
1500
1000
500
0
1200
1400
1600
1800
Raman shift (cm^{-1})

Fig. 2

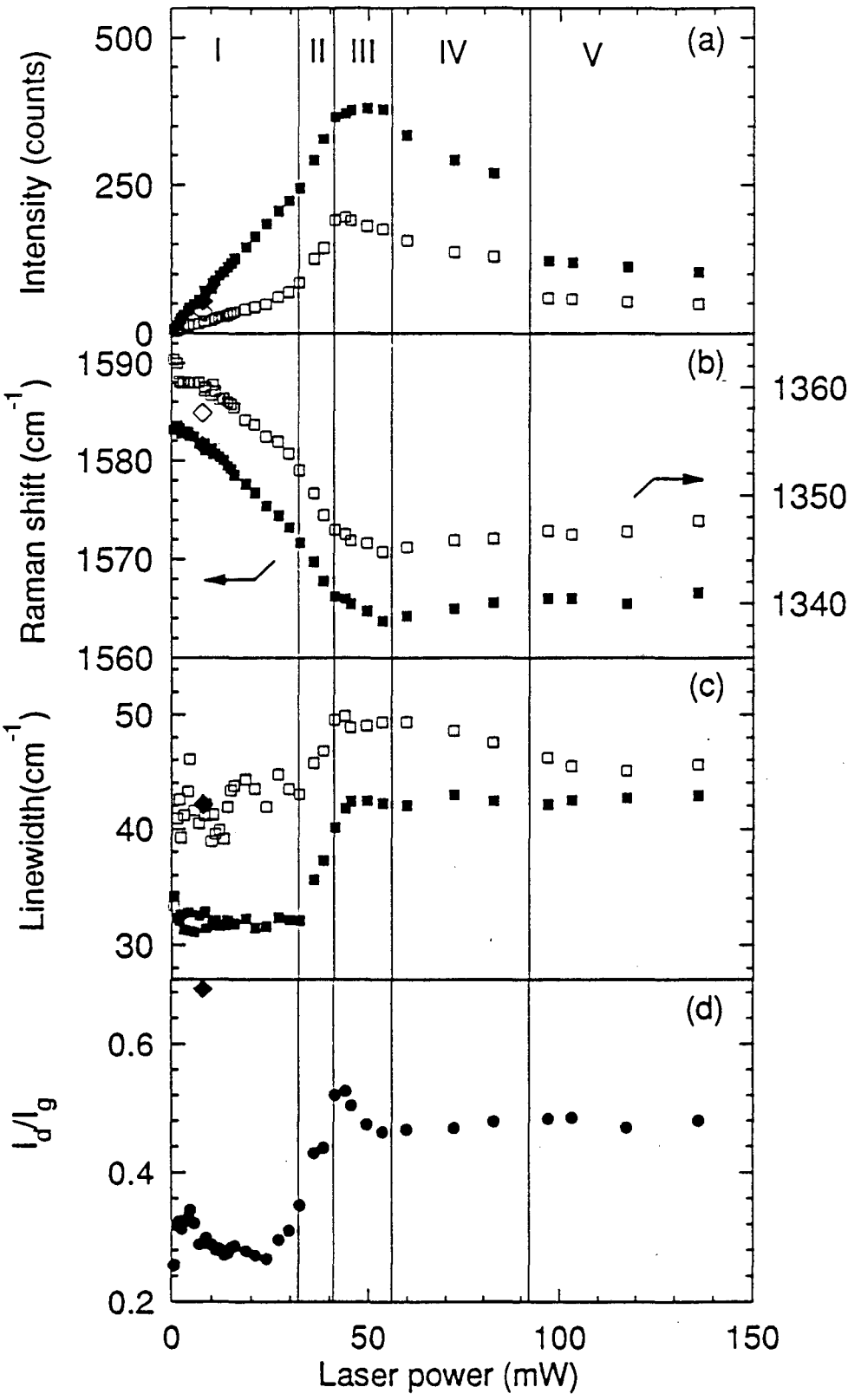
Intensity (counts)
500
250
0
I
II
III
IV
V
(a)
Raman shift (cm^{-1})
1590
1580
1570
1560
(b)
1360
1350
1340
Linewidth(cm^{-1})
50
40
30
(c)
I_d/I_g
0.6
0.4
0.2
(d)
0
50
100
150
Laser power (mW)

Fig. 3

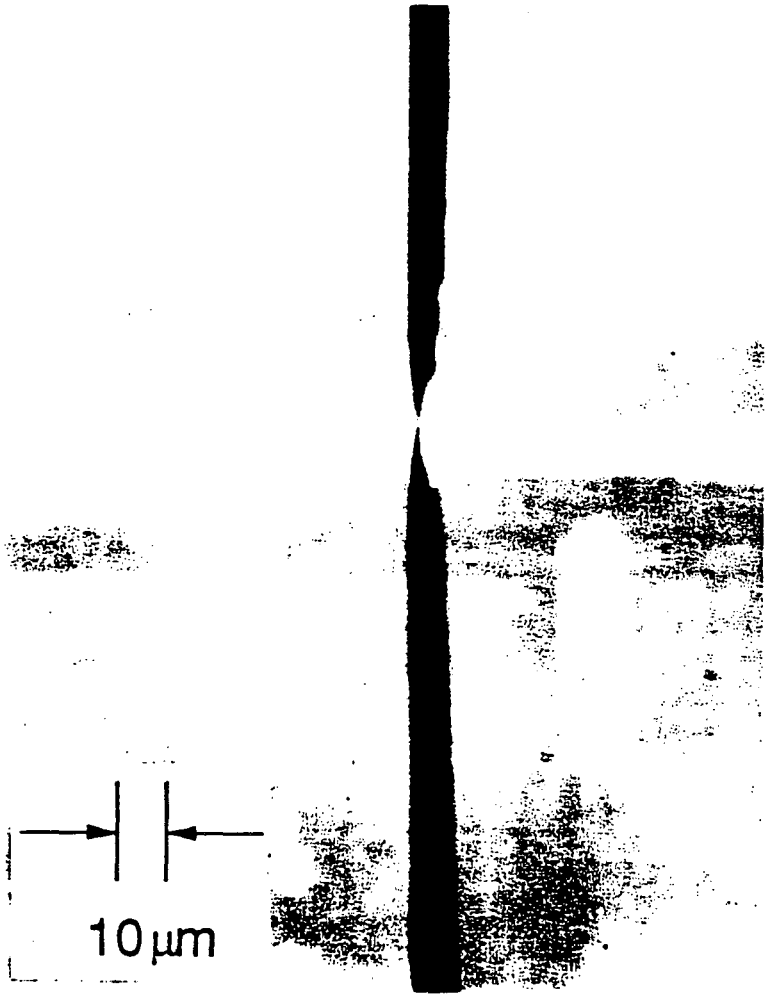

Fig. 4

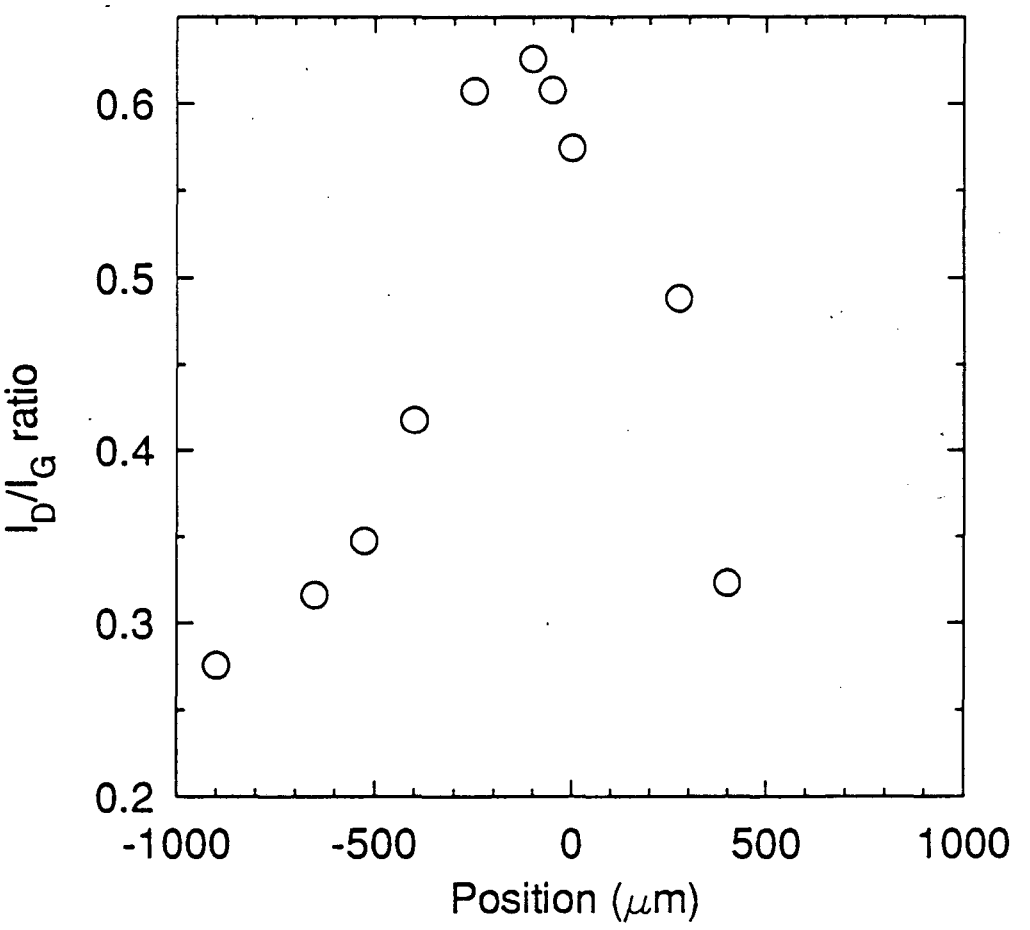

Fig. 6

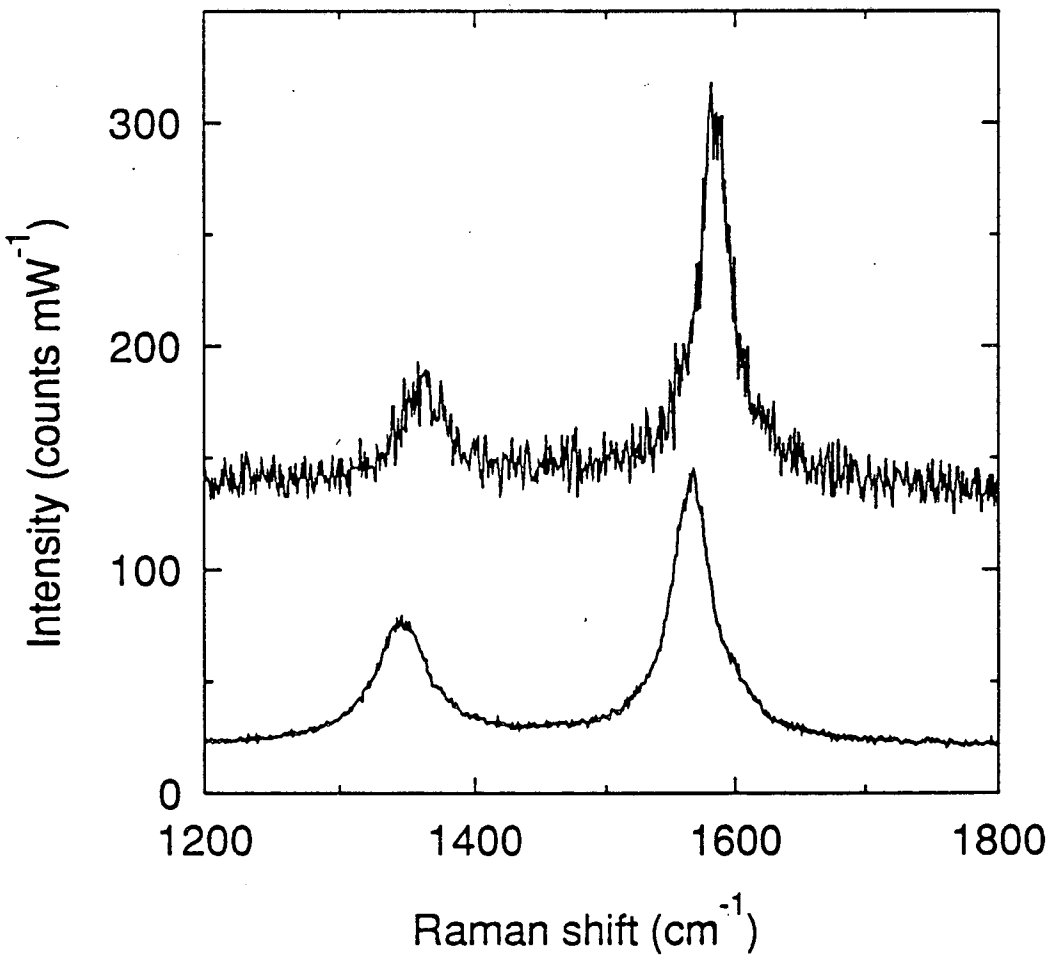
300
200
100
0
Intensity (counts mW^{-1})
1200
1400
1600
1800
Raman shift (cm^{-1})

Fig. 5

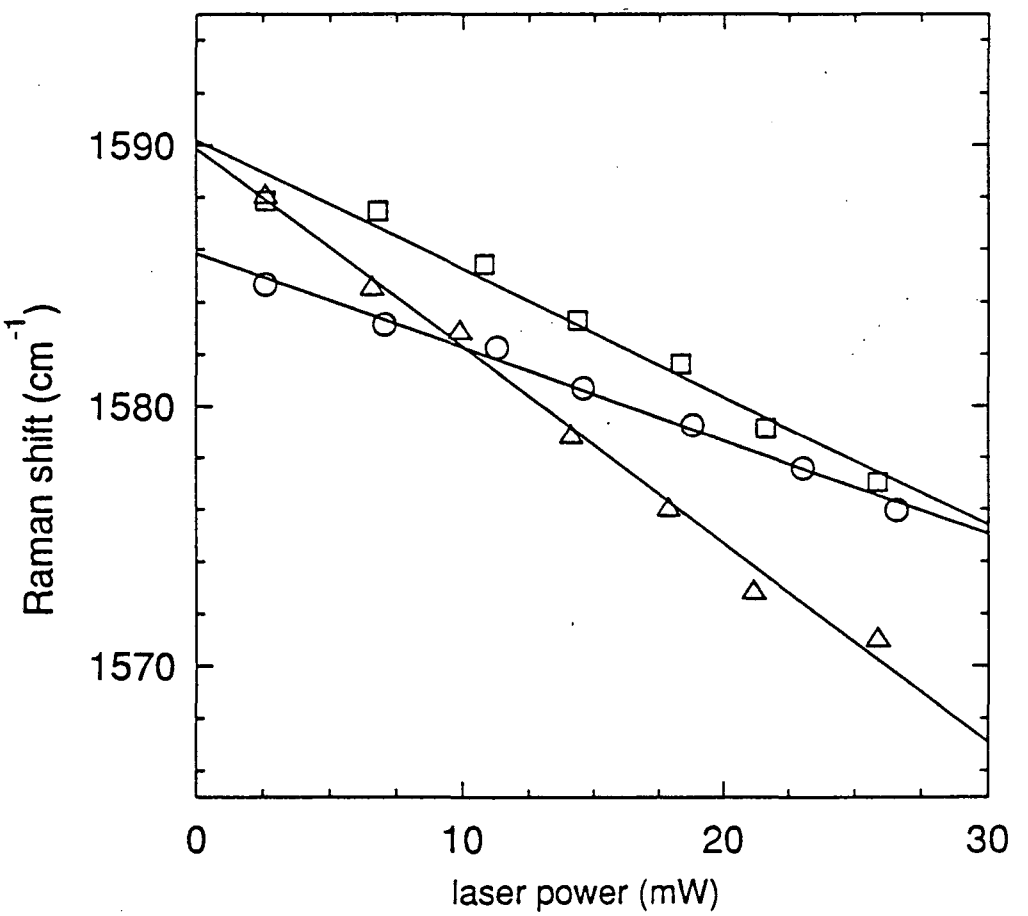

Fig. 7

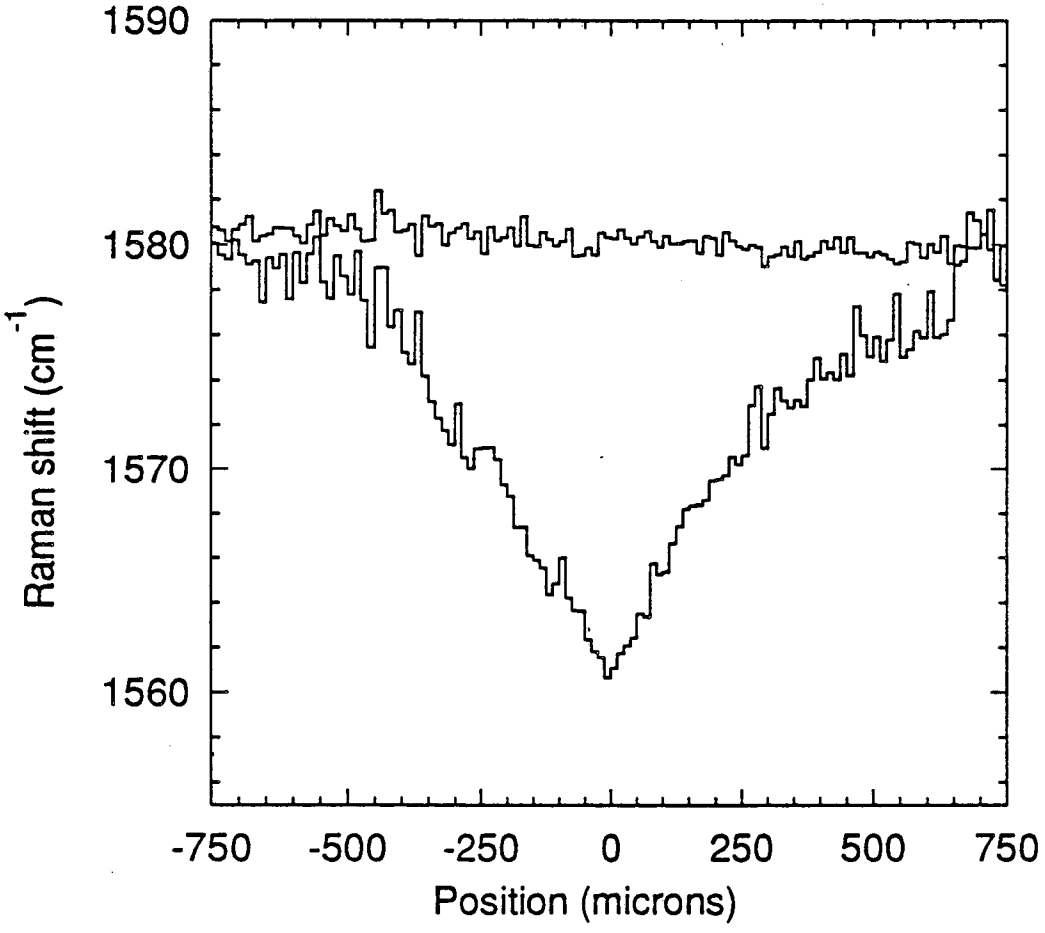
1590
1580
1570
1560
Raman shift (cm^{-1})
-750
-500
-250
0
250
500
750
Position (microns)

Fig. 8

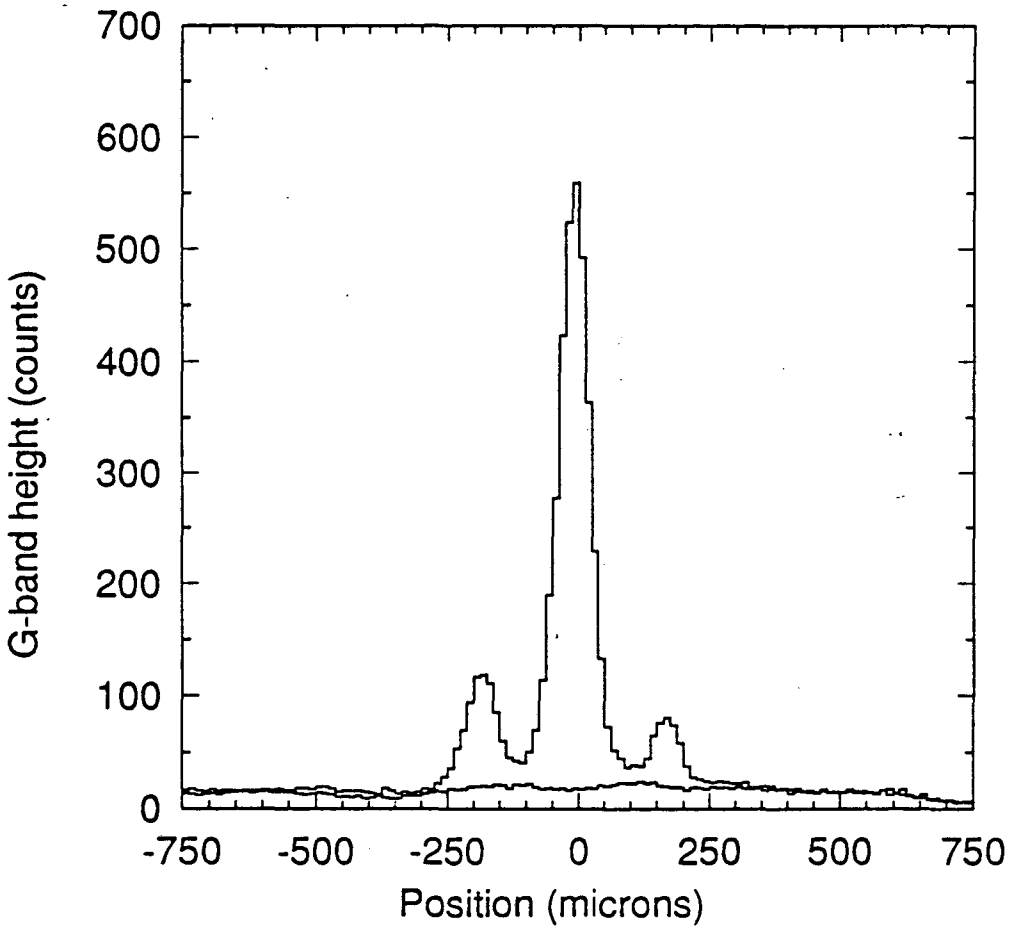
700
600
500
400
300
200
100
0
G-band height (counts)
-750
-500
-250
0
250
500
750
Position (microns)

Fig. 9

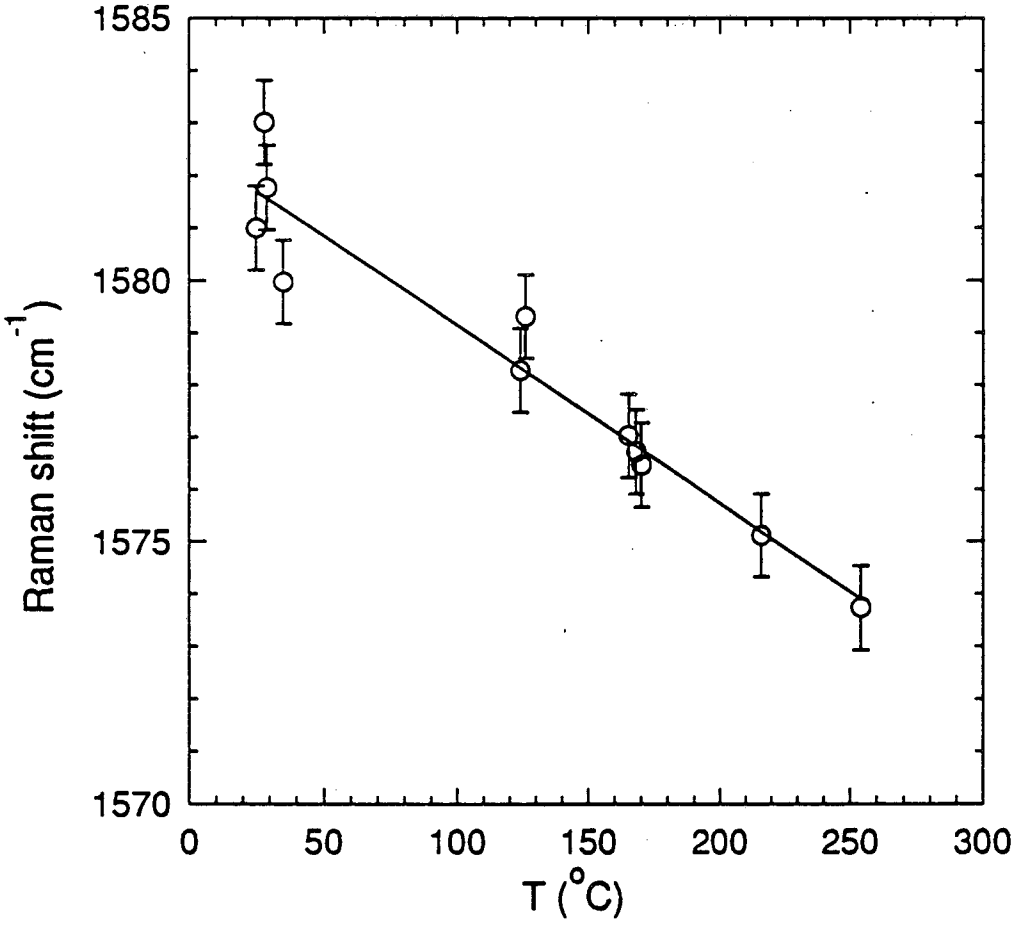
1585
1580
1575
1570
Raman shift (cm^{-1})
0
50
100
150
200
250
300
T (^{o}C)

Fig. 10

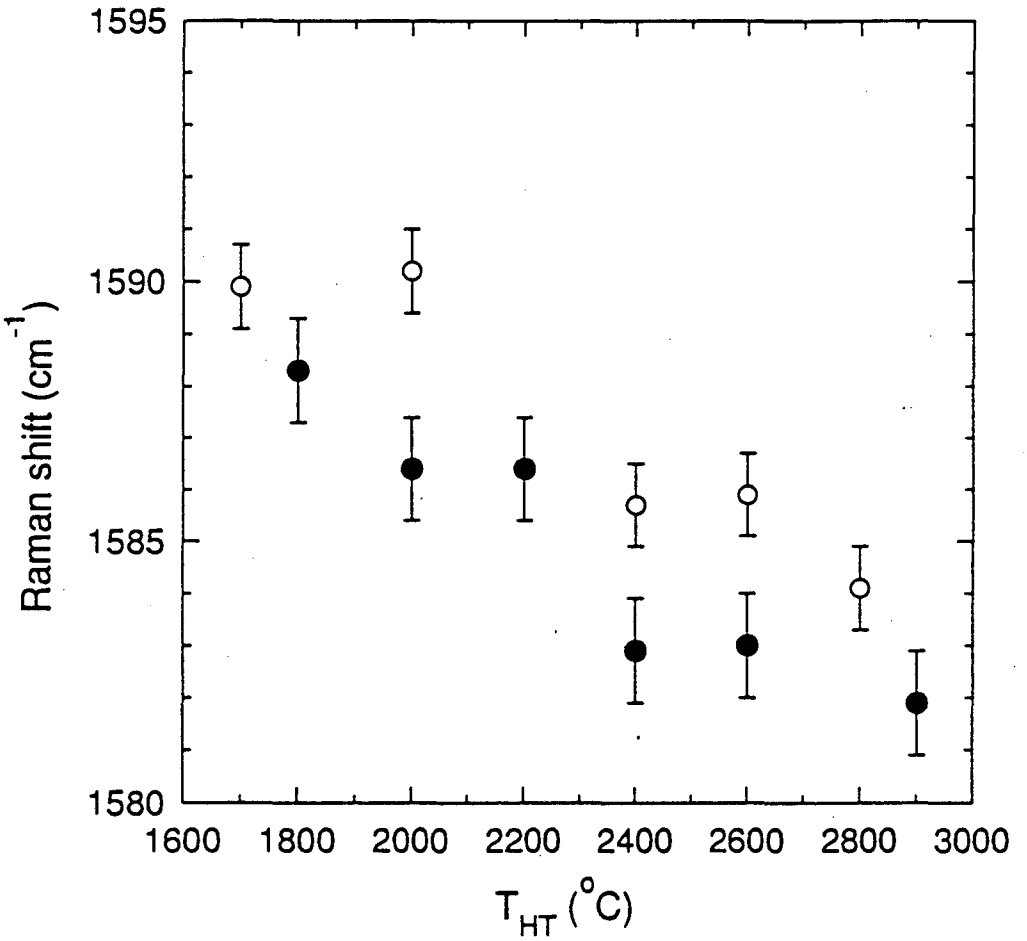
1595
1590
1585
1580
Raman shift (cm^{-1})
1600
1800
2000
2200
2400
2600
2800
3000
T_{HT} (^{o}C)

Fig. 11

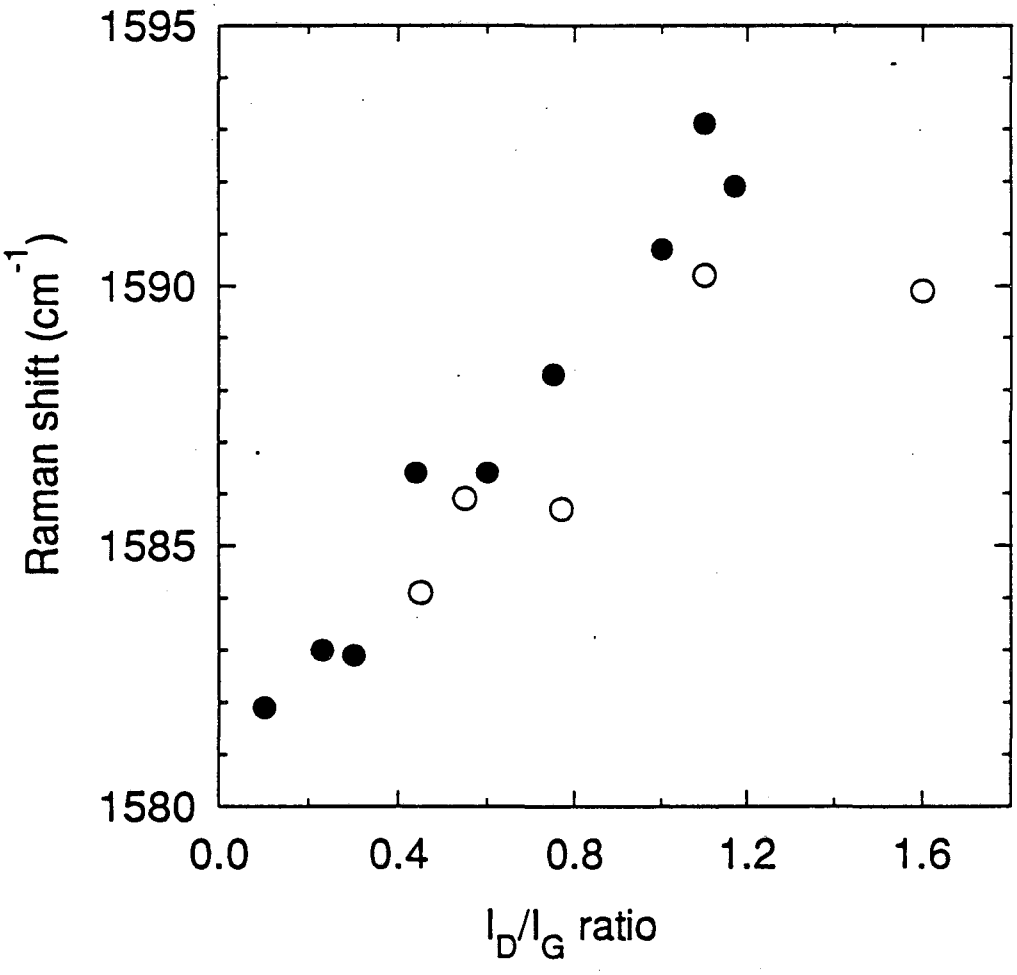

Fig. 12

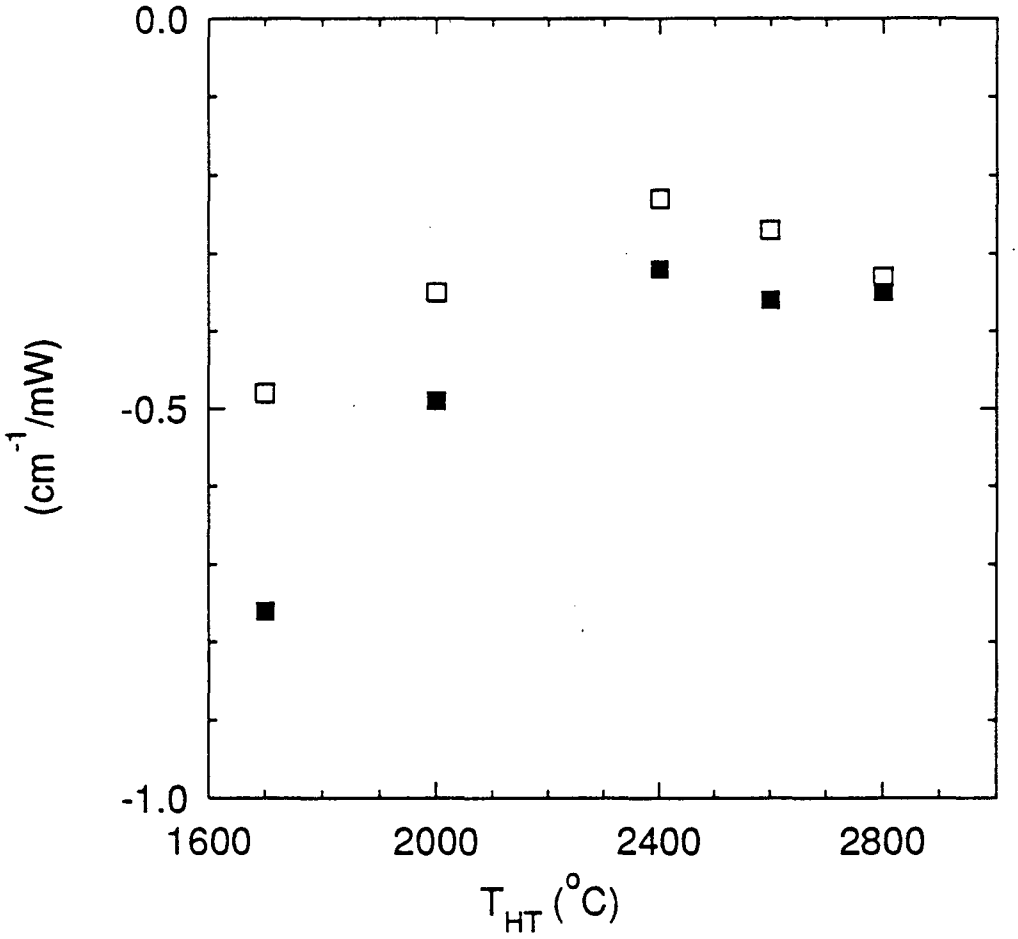

Fig. 13

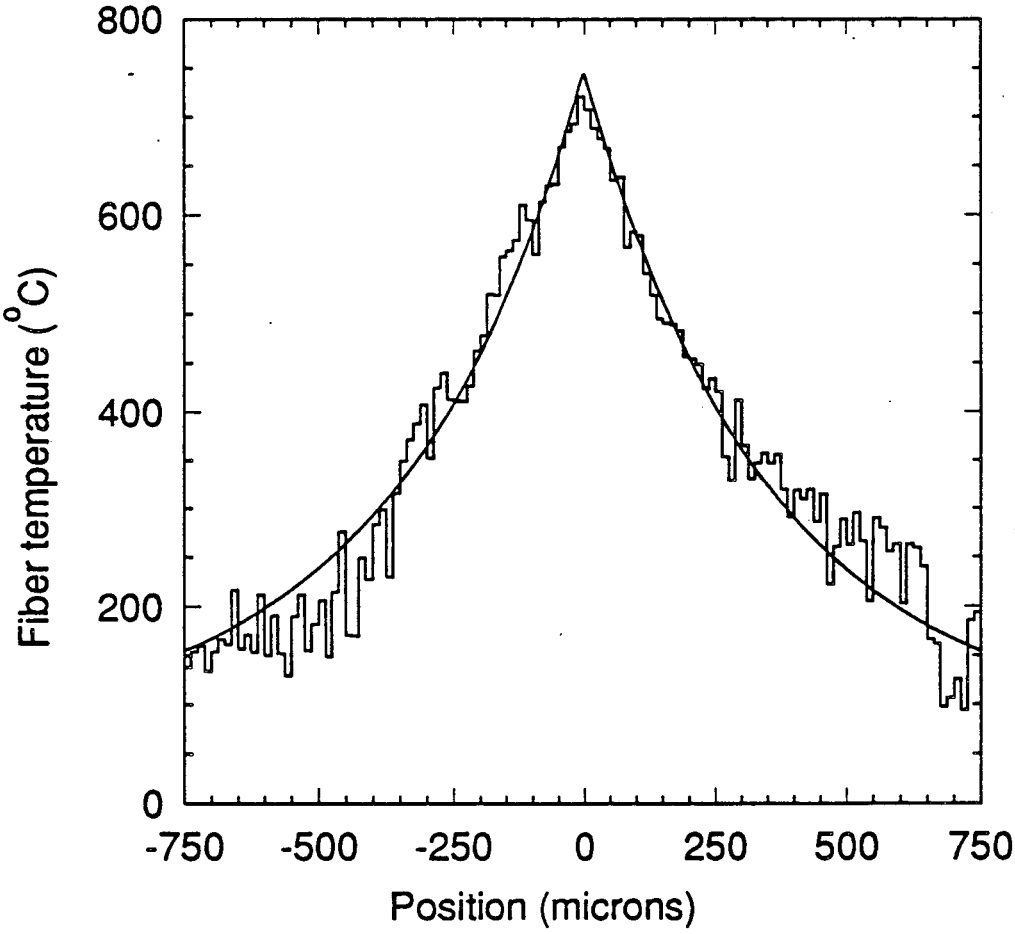
800
600
400
200
0
Fiber temperature (°C)
-750
-500
-250
0
250
500
750
Position (microns)

Fig. 14

LAWRENCE BERKELEY LABORATORY
CENTER FOR ADVANCED MATERIALS
1 CYCLOTRON ROAD
BERKELEY, CALIFORNIA 94720